This document is the accepted manuscript version of the following article:
Berens, M. J., Ulrich, B. A., Strehlau, J. H., Hofstetter, T. B., & Arnold, W. A. (2019). Mineral identity, natural organic matter, and repeated contaminant exposures do not affect the carbon and nitrogen isotope fractionation of 2,4-dinitroanisole during abiotic reduction. Environmental Science: Processes and Impacts, 21(1), 51–62. https://doi.org/10.1039/C8EM00381E

Mineral Identity, Natural Organic Matter, and Repeated Contaminant Exposures do not Affect the Carbon and Nitrogen Isotope Fractionation of 2,4-Dinitroanisole during Abiotic Reduction

Matthew J. Berens[†], *Bridget A. Ulrich*[‡], *Jennifer H. Strehlau*[†], *Thomas B. Hofstetter*[‡], *and William A. Arnold**[,†]

[†]Department of Civil, Environmental, and Geo- Engineering, University of Minnesota, 500 Pillsbury Drive SE, Minneapolis, MN, 55455-0116, United States

[‡]Eawag, Swiss Federal Institute of Aquatic Science and Technology, Department of Environmental Chemistry, Überlandstrasse 133, CH-8600 Dübendorf

*Corresponding author: William A. Arnold; Phone: 612-625-8582; e-mail: arnol032@umn.edu

ABSTRACT

The recent development of insensitive munitions, such as 2,4-dinitroanisole (DNAN), as components of military explosives has generated concern for potential subsurface contamination and created a need to fully characterize their transformation processes. Compound specific isotope analysis (CSIA) has proven to be a useful means of assessing transformation pathways according to characteristic stable isotope fractionation patterns. The C and N isotope fractionation of DNAN associated with abiotic and enzymatic hydrolysis was recently assessed. The extent to which

DNAN isotope fractionation will be affected by other potentially competing transformation pathways known for nitroaromatic compounds (e.g., reduction) and if previous knowledge can be extrapolated to other environmental matrices remains to be understood. Here, we investigated the C and N isotope fractionation and reaction rate constants of DNAN during abiotic reduction mediated by mineral-associated Fe(II) species as a function of mineral type, natural organic matter presence, and repeated exposures to DNAN. Though rate constants varied, N and C apparent kinetic isotope effects (AKIEs) remained consistent across all experiments (averaged values of ^{15}N-AKIE = 1.0317 ± 0.0064 and ^{13}C-AKIE = 1.0008 ± 0.0005) and revealed significant ^{15}N- and minimal ^{13}C- enrichment in agreement with previous work on nitroaromatic compounds. Moreover, the observed fractionation was clearly distinct from trends for abiotic and enzymatic hydrolysis. This study provides a strengthened basis for the use of compound specific isotope analysis as a robust tool for monitoring DNAN degradation in complex environmental matrices as a component of future remediation efforts.

INTRODUCTION

Insensitive munitions have emerged as safer alternatives to traditional explosives such as 2,4,6-trinitrotoluene (TNT) and hexahydro-1,3,5-trinitro-1,3,5-triazine (RDX). The U.S. military has recently begun development of two insensitive munitions formulations (IMX-101 and IMX-104) containing 2,4-dinitroanisole (DNAN).[1] These formulations exhibit a decreased sensitivity to shock and high temperatures relative to traditional munitions and are designed to minimize the risk of accidental detonations during handling and storage.[2,3] Previous contamination by traditional munitions at military installations has caused concern for future contamination by insensitive munitions, motivating considerable effort towards understanding their subsurface fate and transport properties. Limited data, however, is available concerning the fate and transport of these new energetic materials.[4,5] Moreover, the toxicity and sediment-water partitioning behavior of DNAN and its transformation products have shown to be similar to that of TNT.[1,6,7] A better understanding of the relevant natural attenuation processes for DNAN in subsurface environments is therefore needed.

The degradation of DNAN in the environment occurs through several abiotic transformation pathways including alkaline hydrolysis[8,9], photolysis,[10,11] and also reduction in systems containing zero valent iron or other iron-bearing mineral species.[12,13] Previous work has shown that ferrous iron associated with iron oxides, iron (oxy)hydroxides, and sulfide-bearing minerals mediates the abiotic transformation of nitroaromatic compounds (NACs) under anoxic conditions,[14–17] reducing NACs to the corresponding substituted anilines (e.g., Scheme 1).[18,19] Such pathways have been observed for DNAN and can be attributed to mineral-bound Fe(II) species as well as electron-donating functional groups of natural organic matter.[15,20] Substituted anilines may also form during biotic processes facilitated by Fe(III)-reducing microorganisms and other concomitant suites of

aerobic and anaerobic microbiota.[4,20–24] Complete reduction of DNAN in subsurface environments is often achieved through coupled abiotic-biotic transformation mechanisms. For example, Niedźwiecka et al.[25] observed rapid DNAN reduction in microcosms containing Fe(III) following reduction of Fe(III) to Fe(II) by *Geobacter metallireducens*, compared to microcosms without ferric iron.

Scheme 1. Reductive transformation pathway of DNAN, with one N atom at which the reduction reaction can occur highlighted. The pathway is initiated by the formation of a nitroso-moiety **(2)** from a NO_2 group,[13,20,26] followed by formation of hydroxylamine **(3)** and subsequently an amine derivative (e.g., 2-methoxy-5-nitroaniline (MENA) **(4)**). The mechanism of aromatic NO_2 reduction is shown here arbitrarily for the *ortho*-substituent and does not imply preferential formation of MENA. However, most current studies are in agreement that reduction is initiated at the *ortho* substituent.[20,26,27] In the presence of sufficient reductant, this process continues through other intermediates before reducing the second NO_2-group to generate 2,4-diaminoanisole (DAAN) **(5)**.[15]

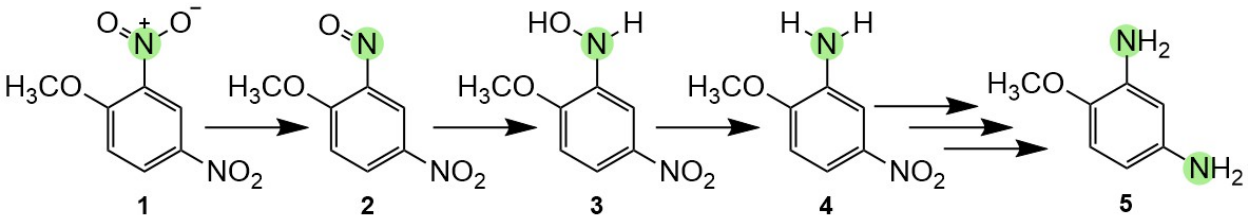

Assessing the transformation of NACs in the environment is complicated by the possibility of several simultaneous (and potentially competing) transformation and transport processes (e.g., sorption, volatilization, (bio)degradation).[4] Likewise, NACs in the subsurface may be present in different phases[7,28] and exhibit high soil and sediment sorption, rendering the interpretation of concentration dynamics difficult.[29,30] Compound specific isotope analysis (CSIA) has proven useful for assessing degradation processes of NACs in such complex environmental systems with potentially competing attenuation processes.[31,32] CSIA of NAC (bio)transformations is based on characteristic changes in stable isotope ratios (e.g., $^{15}N/^{14}N$, $^{13}C/^{12}C$) that are indicative of a specific

pathway.[33,34] Thus, it is possible to use CSIA to determine the reaction process occurring without the need to detect reaction products, which may be not be amenable to detection, further degraded, bind to organic matter, or sorb to the matrix.[35,36] These so-called isotope fractionation patterns arise from apparent kinetic isotope effects (AKIEs) controlled by changes in the bonding environment at the reactive position during the initial stages of NAC transformation.[37] Indeed, AKIEs have been well-characterized for the abiotic reduction of several NACs including chloro- and methyl-substituted nitrobenzenes, dinitrobenzene isomers, and 2,4,6-trinitrotoluene (^{15}N-AKIE ~ 1.03–1.04, ^{13}C-AKIE ~ 1.001).[38–41]

Abiotic reductions of NACs (Scheme 1) result in large primary ^{15}N-AKIEs, for which cleavage of the first N—O bond to form a nitroso intermediate is the rate-limiting step and thus dictates shifts in the isotope signature. In contrast, the corresponding ^{13}C-AKIEs are typically small because C atoms are not directly involved in the rate-limiting step (i.e., secondary AKIEs).[38–40] Whereas Ulrich et al.[42] recently assessed ^{13}C and ^{15}N fractionation during the abiotic (i.e., alkaline) and enzymatic hydrolysis of DNAN, the isotope fractionation that arises from reductive transformation of DNAN remains to be assessed. Previous work on the abiotic reduction of NACs by Fe(II) associated with the surfaces of iron oxides and clay minerals suggests that DNAN will display similar isotopic fractionation behavior.[38–41] Those studies, however, focused on isomers of chloro- and methyl-substituted compounds and on a limited set of minerals (i.e., Fe(II) associated with goethite and structural Fe(II) in magnetite and ferruginous smectite). Showing that fractionation is independent of environmental matrix conditions is imperative for accurately quantifying the extent of pollutant degradation at contaminated field sites where the subsurface composition may be complex, changing, or unknown. Potential matrix conditions could include the presence of different minerals with different reactivity towards NACs, interferences of natural organic matter

(NOM) through association with the mineral surface, and the transformation of Fe minerals after repeated exposure to NACs. Previous work has revealed that transformation rates of NACs may span orders of magnitude depending on the type of mineral involved owing to modulations in the electrochemical potential (E_H) of the oxide-associated Fe(II) system.[14,16,43–45] The presence of NOM may also impact reaction rates through the formation of Fe(II)-NOM complexes.[46] NOM may also alter particle dispersion or change the availability of reactive sites.[47–50] Repeated contaminant exposure may induce evolution of the mineral structure, potentially interfering with Fe(II) uptake or developing a new surface oxide.[50,51] Because the magnitude of isotope fractionation during the reduction of NACs was proposed to be determined by changes of bonding in the aromatic NO_2 substituent(s) regardless of the rate of transformation (i.e., reduction of a nitro-group to form a nitroso-moiety), we hypothesize isotope fractionation associated with the reduction of new potential contaminants such as DNAN in the environment will be consistent with previously determined AKIE-values as well as independent of matrix conditions discussed above.[31,38,40,41,52,53]

The goal of this study was to investigate the effects of matrix conditions that could be encountered in environmental systems on the reaction kinetics and C and N isotope fractionation associated with abiotic DNAN reduction, thereby evaluating the robustness of AKIEs and the associated isotope enrichment factors for the application of CSIA for assessing reductive transformations of DNAN. To this end, we characterized the pseudo-first-order kinetics and the C and N isotope fractionation during abiotic DNAN reduction as a function of (1) the type of mineral (goethite, magnetite, or mackinawite), (2) the presence of natural organic matter (NOM), and (3) repeated exposures to DNAN. Measured C and N isotope signatures ($\delta^{13}C$ and $\delta^{15}N$) as a function of reaction extent were used to derive the corresponding isotope enrichment factors (ε_C and ε_N) and apparent kinetic isotope effects (^{13}C-AKIE and ^{15}N-AKIE). These values were

compared to previous evidence on isotope effects associated with NAC reduction as well as to those recently established for alkaline and enzymatic hydrolysis[42] to confirm the efficacy of CSIA to distinguish between the most likely environmental DNAN degradation reactions. The findings of this work provide a strengthened basis for identifying and assessing these processes in subsurface environments by CSIA, a result that will be of particular significance to potential future efforts to monitor and remediate DNAN-contaminated subsurface environments.

METHODS

Chemicals

Detailed chemical information is provided in the Electronic Supplementary Information (ESI, Section S1.1). Fresh Fe(II) and DNAN stock solutions were prepared prior to each reduction experiment. Aqueous Fe(II) stock solutions were prepared by adding 0.44 g $FeCl_2 \cdot 6H_2O$ to 0.4 mL of 1 M HCl and enough deoxygenated ultrapure water to achieve a final concentration of 175 mM. DNAN (Alfa Aesar, 98%, CAS# 119-27-7) stock solutions were similarly prepared in deoxygenated methanol. It should be noted that DNAN was purchased in 2016 and is no longer available from Alfa Aesar in the United States. DNAN transformation products 2-methoxy-5-nitroaniline (MENA, 98%, CAS# 99-59-2) and 2,4-diaminoanisole (DAAN, ≥98%, CAS# 615-05-4) were purchased from Fisher Scientific. Elliot Soil humic acid (ESHA) was purchased from the International Humic Substances Society (IHSS, St. Paul, MN). With the exception of goethite synthesis and storage, all experiments were performed inside an anaerobic chamber (Coy, 95% N_2/5% H_2).

Mineral Synthesis

Detailed mineral synthesis and analysis procedures are provided in Section S2. Mackinawite was precipitated using the method of Butler and Hayes[54] and particles were stored in suspension in the anaerobic chamber at room temperature and pH 7. Synthetic goethite was prepared according to Anschutz and Penn[55] and stored in suspension outside the anaerobic chamber at pH 4 and 4 °C. Magnetite synthesis was adapted from Schwertmann and Cornell.[56] Synthetic magnetite was dried and stored as a powder inside the chamber. Magnetite stoichiometry (x = Fe(II)/Fe(III)) was determined by acid dissolution in 3 M HCl (Sigma, trace metals) as $x = 0.50$. Total Fe(II) and Fe(III) content was quantified using the ferrozine colorimetric assay (Section S1.2).[57] Each mineral was characterized by X-ray diffraction (XRD) and compared to reference patterns to support the presence of each desired mineral phase (Figure S1). The XRD results for synthetic magnetite and goethite indicated the presence of only the desired phases. The pattern collected from mackinawite contained peaks consistent with mackinawite and greigite (Fe_3S_4, PDF No. 16-0713). Previous work has reported rapid phase transformation of mackinawite to greigite under oxic conditions at room temperature, which may suggest the presence of greigite as an artifact of sample preparation.[58]

Mineral surface areas were determined by nitrogen adsorption analysis using the Brunauer-Emmett-Teller (BET) adsorption model[59] as 103.8 m^2/g and 17.8 m^2/g for goethite and magnetite, respectively. Mackinawite decomposed under high vacuum and temperature during outgassing and an accurate surface area measurement could not be obtained. Mass loading experiments were performed and the particle concentrations in goethite and mackinawite suspensions were approximately 10 g/L and 33 g/L, respectively.

Batch Reactions

Batch experiments to assess reaction kinetics were performed in triplicate in 50 mL borosilicate serum bottles capped with Teflon-lined butyl rubber septa. All reactors contained a mineral suspension in $NaHCO_3$ buffer (10 mM, pH 7.0). Mineral loadings were 2.0 g/L for magnetite, 1.5 g/L for mackinawite, and 1.0 g/L for goethite. Aqueous Fe(II) was added to goethite and magnetite reactors at a concentration of 1 mM and equilibrated overnight by rotating on an end-over-end rotator (Glas-Col, 40 rpm). No Fe(II) was added to mackinawite reactors and only a 1 h equilibration was performed. For the subset of reactions containing NOM, ESHA was added at 5 mg C/L prior to equilibration. The pH was then measured and Fe(II) concentrations were determined using the ferrozine method.[57] If necessary, the pH was adjusted back to 7.0 with 1 M HCl or 1 M NaOH (Fisher, ACS grade) and the Fe(II) was augmented to 1 mM in the magnetite and goethite reactors. Reactions were initiated by spiking DNAN from the methanolic stock solution to a concentration of 0.20 mM and returning reactors to the rotator. The DNAN concentration was selected to ensure that a sufficient concentration remained in solution to allow detection by CSIA after achieving our target of 95% reduction. Every hour, the pH and Fe(II) in the reactors were determined and adjusted to pH 7 and 1 mM, respectively. This was necessary because the initial 1 mM Fe(II) is not sufficient to completely reduce the 0.20 mM DNAN (a minimum of 2.4 mM e^- is needed to reduce both $–NO_2$ moieties to $–NH_2$), and it allows for the assumption of pseudo-first-order kinetics by maintaining a high Fe(II) concentration. At appropriate time points, an aliquot from each reactor was removed and filtered with a 0.2 μm PTFE syringe filter. Aqueous DNAN, MENA, and DAAN concentrations were quantified at a wavelength of 230 nm using an Agilent 1200 series high pressure liquid

chromatograph (HPLC, method in Section S1.3). Pseudo-first-order rate constants were determined by regression using a log-linear relationship of $\ln(c/c_0)$ versus time.

To perform batch experiments for CSIA, eight replicate reactors were assembled as described above for each set of reaction conditions. At each sampling point, the entire contents of one reactor were removed, filtered, and stabilized by adjusting the pH to < 4 with 1 M HCl (Sigma, trace metals). Approximately 14 mL of acidified filtrate were transferred to a clean 20 mL glass vial, fitted with a butyl rubber plug (Fisher, 20 mm) and crimp cap, and stored at 4 °C until isotope analysis (method described below).

To assess the baseline reactivity of each mineral suspension for DNAN transformation, reactors were assembled containing only mineral, buffer, Fe(II) (for iron oxides), and DNAN. A control was performed with Fe(II) alone in $NaHCO_3$ buffer, in which no reaction was observed over 21 days (Section S3). To perform repeated contaminant exposure experiments, batch reactors were assembled in triplicate as described above. The first spike was initiated by injecting DNAN to a concentration of 0.20 mM. The Fe(II) content was determined in goethite and magnetite reactors after 1 h of reaction and adjusted accordingly to return each reactor to 1 mM Fe(II). A single aliquot (~0.20 mL) was removed for analysis by HPLC after approximately 8 h to confirm complete DNAN transformation (<0.001 mM). Subsequently, to avoid the formation and accumulation of products over multiple reaction cycles, the aqueous solution from each reactor was removed and replaced with fresh buffer solution at the end of each reduction cycle. Suspensions were settled for at least 12 h or, in the case of magnetite, particles were isolated by using a neodymium magnet and discarding the supernatant. Fresh Fe(II) (1 mM) was added to goethite and magnetite reactors and the reactors were then equilibrated as described above. The pH was adjusted back to 7.0 in all reactors and a second DNAN spike was initiated

and the reaction performed as described above. This procedure was carried out for five cycles, with concentrations measured as a function of time in triplicate during the desired cycle. For CSIA, a reactor was sacrificed at each time point during the fifth cycle and prepared for isotope analysis as described above.

Compound Specific Isotope Analysis

Isotopic analysis of DNAN was conducted by gas chromatography isotope ratio mass spectrometry (GC/IRMS). DNAN was concentrated by solid phase micro extraction (SPME) prior to isotopic analysis. A method was modified from established SPME procedures[42,60] using the PAL SPME Arrow (DVB/PDMS sorption phase, 120 μm phase thickness, 1.1 mm diameter) instead of a normal SPME fiber, such that improved sensitivity could be obtained with a larger sorption phase.[61] Automated SPME was carried out using a PAL autosampler equipped with a PAL SPME Arrow Tool and a Heatex Stirrer. All samples were initially diluted with 10 mM phosphate buffer (pH 7, prepared with nanopure water) to obtain concentrations within a range of linear response, and sodium chloride (100 g/L) was added to maximize extraction efficiency. Following equilibration at 50 °C for 10 min, the SPME Arrow was immersed in the sample for 70 minutes at 50 °C (600 RPM stir rate), and then DNAN was thermally desorbed from the arrow in an injector equipped with a deactivated liner (270 °C, 6 minutes).

DNAN $^{15}N/^{14}N$ and $^{13}C/^{12}C$ ratios were determined using a Trace GC (Thermo Electron Corp.) coupled to an IRMS (DeltaPLUS XL, Thermo Electron Corp.) via a combustion interface (GC Combustion III, Thermo) equipped with a custom-made Ni/Pt reactor. The GC contained an Rtx-5MS capillary column (0.32 mm ID, 1 μm film thickness, 30 m length) and was operated in splitless mode (splitless time 6 minutes, purge flow 50 ml/min) with the following temperature program: 50 °C for 1 minute, ramp 10 °C/min to 250 °C, hold for 5 minutes. During $\delta^{15}N$

241 analysis a liquid nitrogen trap was used to trap CO_2 produced from combustion. The oxidation
242 reactor was operated as described previously.[62] Method quantification limits (MQLs) for $\delta^{13}C$ and
243 $\delta^{15}N$ according to the moving mean procedure were 0.2 μM and 1 μM, respectively.[63]
244 Isotope ratios were references against standard laboratory gases as well as DNAN of known
245 isotopic composition ($\delta^{13}C$ = 37.3 ± 0.1 ‰ and $\delta^{15}N$ = -2.4 ± 0.1 ‰ as determined by an
246 elemental analyzer) using standard bracketing procedures.[64] Carbon and nitrogen isotope
247 enrichment factors (ε_C and ε_N) were derived according to methods described by Pati et al.[64] Linear
248 regression analyses of the isotope signature data were carried out using the log-linearized form of
249 eq. 1:

250 $$\frac{\delta^{h}E+1}{\delta^{h}E_0+1}=\left(\frac{c}{c_0}\right)^{\varepsilon_E} \quad (1)$$

251 where $\delta^{h}E_0$ is the C or N isotope signature of unreacted DNAN and c/c_0 is the fraction of
252 remaining substrate (detailed calculations in Section S4.1).[65] Apparent kinetic isotope effects (^{13}C-
253 AKIE and ^{15}N-AKIE) were then derived from the calculated ε_E values using eq. 2.[32]

254 $$^{h}E\text{-AKIE}=\frac{1}{1+z\cdot\varepsilon_E/1000} \quad (2)$$

255 where z is the number of competing reactive sites (i.e., z = 2 for N and z = 1 for C in DNAN).[66]
256 Combined AKIEs were calculated for all three sets of conditions for each mineral phase (i.e.,
257 mineral alone, presence of NOM, repeated contaminant exposures) according to the method of
258 Scott et al.[67] using the Pitman estimator. Additional details for isotope analysis are provided in
259 Section S4.
260

RESULTS AND DISCUSSION

Kinetic Experiments.

Pseudo-first-order rate constants (k_{obs}) from triplicate reactors were calculated for all conditions tested (Table 1). The only reaction products observed were MENA and DAAN. Aqueous concentrations of DNAN and its transformation products are highlighted in Figure 1. Mass balances were ~80%, and given the high initial concentration, the incomplete mass balance could be due to formation of coupling products between hydroxylamine and nitroso intermediates.[68,69] The limited accumulation of DAAN is likely due to lower reactivity of MENA compared to DNAN, because Fe(II) was maintained at 1 mM throughout the experiments with goethite and magnetite. The greater accumulation of MENA with mackinawite may be due to changing mineralogy (see below). Because the focus of CSIA analysis was on DNAN, monitoring the reaction to complete conversion to DAAN was not necessary. The highest transformation rates were observed for the first contaminant exposure (i.e., Spike 1) in Fe(II)/goethite suspensions followed by mackinawite and Fe(II)/magnetite, respectively. Aqueous Fe(II) was supplemented (and added throughout the experiment to maintain a 1 mM concentration) into goethite and magnetite suspensions because these minerals contain little to no inherent surface associated Fe(II) reactive sites. In contrast, mackinawite is an Fe(II)-bearing mineral known to directly participate in reduction reactions.[54,70,71] Mineral concentrations in batch reactors decreased in the order of magnetite (2.0 g/L), mackinawite (1.5 g/L), and goethite (1.0 g/L), resulting in the same order of increasing k_{obs} when normalized to mineral loadings. Mineral concentrations were selected such that DNAN reduction experiments occurred within a similar experimental time frame. Organic matter (5 mg C/L from ESHA) had no effect on k_{obs} in all samples tested. Previous work has shown that organic matter decreases reduction rates of NACs,

likely via competitive adsorption with Fe(II) or blocking of reactive sites at the mineral surface.[50] One possible explanation for these differences is that our work uses higher mineral loadings and a constant supply of Fe(II), thus increasing the abundance of Fe(II) and mineral reactive sites while decreasing the competition for each. Alternatively, higher mineral loadings and Fe(II) content may overcome any increases in E_H imposed by NOM functional groups which have been linked to decreased rates of contaminant reduction.[45]

Table 1. Pseudo-first-order rate constants, k_{obs}, for DNAN reduction.[a,b] Rate constants were calculated in systems containing the mineral alone (Spike 1), the addition of NOM (ESHA), and during the fifth sequential contaminant exposures (Spike 5).

System	Mackinawite	Goethite	Magnetite
	k_{obs} (h^{-1})		
Spike 1	1.15 ± 0.12	2.55 ± 0.14	0.79 ± 0.05
ESHA	1.16 ± 0.09	2.49 ± 0.18	0.82 ± 0.04
Spike 5	0.19 ± 0.04	2.52 ± 0.11	0.81 ± 0.07

[a]Rate constants obtained from linear regression of natural log of concentration versus time data. [b]Uncertainties represent standard deviations of triplicate reactors.

Rate constants calculated during repeated contaminant exposure experiments revealed that reaction kinetics were independent of previous contaminant exposure in reactors containing goethite and magnetite. This is consistent with previous work with iron oxides, confirming that minimal variation in the rate constant can be expected if pH is carefully maintained over multiple contaminant exposures.[50] Moreover, these results suggest that any mineral transformations that may have occurred during repeated exposures did not significantly affect the reduction potential of the oxide-bound Fe(II) in each system.[45]

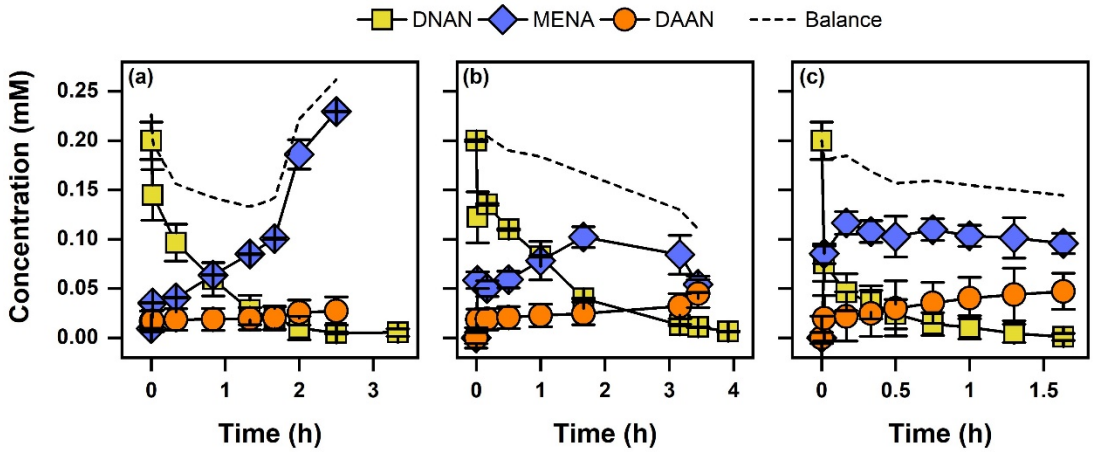

Figure 1. Aqueous concentrations of DNAN, MENA, and DAAN during DNAN kinetics experiments in suspensions of (a) mackinawite (1.5 g/L), (b) magnetite (2 g/L), and (c) goethite (1.0 g/L). Reactions were performed at pH 7 with 1 mM Fe(II) and are for the first spike of DNAN. Error bars represent standard deviations of triplicate reactors. Dotted lines represent mass balances (moles) of the three compounds.

In contrast to goethite and magnetite, the observed pseudo-first order reaction rate constant for mackinawite decreased with each exposure to DNAN (Figure 2a). This observation could be attributed to the development of lepidocrocite (γ-FeOOH, PDF No. 44-1415) over the course of five contaminant spikes (Figure 2b). While it is likely the rate constant was changing over the course of each contaminant exposure, a pseudo-first order model adequately fits the data for each spike and allows quantification of the loss of reactivity over time (Figure 2a). Lepidocrocite is a polymorph of goethite and could be expected to exhibit similar reactive properties to goethite if sufficient Fe(II) was available,[43] which it likely is not in this system given that none was added.

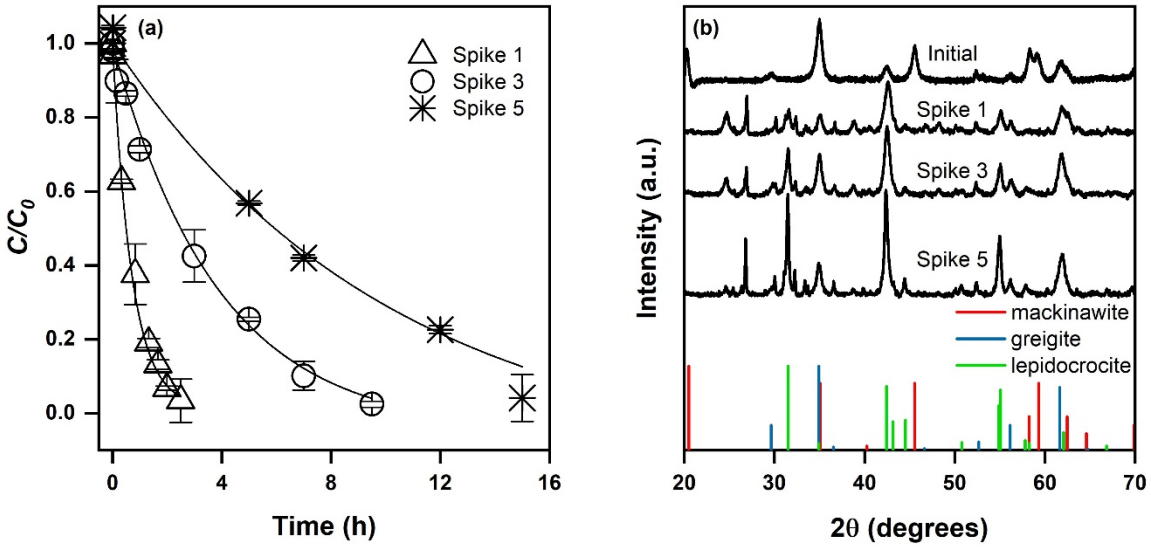

315

316 **Figure 2.** (a) Kinetic profiles and (b) XRD patterns of mackinawite reactions during repeated exposures to
317 DNAN. Error bars represent standard deviations of triplicate reactors, and lines are pseudo-first order fits
318 to the data.

319

320 Therefore, the observation that k_{obs} decreases during lepidocrocite formation is supported by
321 the observation that lepidocrocite has a lower k_{obs} for NAC transformation and the requirement of
322 Fe(II) supplementation for reaction to occur on Fe(III)-oxides.[14] These results highlight the
323 importance of understanding the effects of phase evolution on reaction kinetics at highly
324 contaminated sites.

325 **CSIA of DNAN reduction**

326 The transformation of DNAN in suspensions of mackinawite, Fe(II)/goethite, and
327 Fe(II)/magnetite was associated with strong enrichment of ^{15}N of up to 60‰ in the remaining
328 substrate whereas enrichment of ^{13}C was minimal (below 2.4‰) in agreement with previous work
329 on the reductive transformation of other NACs.[33,34,37,38,41] The extent of DNAN degradation was
330 related to isotope fractionation by eq. 1. Average ε_N-values for the reduction of DNAN derived
331 after the first vs. fifth spike to the mineral suspension decreased by 1‰ to 5‰ as shown in Table

2 (e.g., -19 ± 1‰ in mackinawite experiment spike 1 vs. -16 ± 2‰ for spike 5). All changes, however, were within the uncertainty (95% confidence intervals). Variations of ε_C were much smaller (with errors of the same magnitude as the measurements) and did not show a discernable trend (Figure 3b). The minimum and maximum ^{15}N-AKIE-values derived from ε_N (eq. 2) ranged from 1.018 ± 0.002 (magnetite, spike 5) to 1.039 ± 0.001 (mackinawite, spike 1) and fall within the range of data reported for the abiotic reduction of substituted mono-, di-, and trinitroaromatic compounds by mineral-bound Fe(II) reported previously.[33,34,37,38,41] Whereas large ^{15}N-AKIEs are due to the rate-limiting cleavage of the first N–O bond of the aromatic NO_2 groups, ^{13}C-AKIE are small (i.e., secondary) vary between 1.000 and 1.002 (Table 2) because no changes in bonds to C occur. Identical observations were made with experiments where DNAN was reduced in mineral suspension in the presence of ESHA in that ^{15}N- and ^{13}C-AKIE were identical within experimental error to experiments without humic acids.

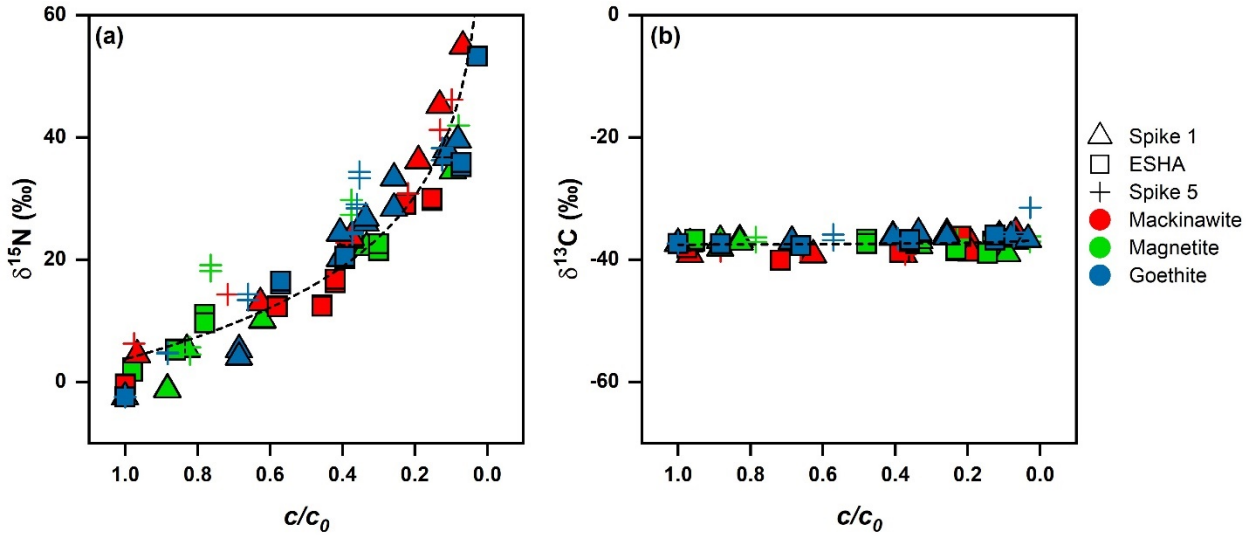

345

346 **Figure 3.** Nitrogen and carbon isotope fractionation of DNAN during abiotic reduction. (a) $\delta^{15}N$ and (b)
347 $\delta^{13}C$ vs. fraction of remaining substrate (c/c_0) with dotted lines provided to guide the eye along the data.
348 Detailed N and C enrichment values are provided in Table 2 (see Figures S3 for $\delta^{15}N$ and $\delta^{13}C$ vs. c/c_0 data
349 separated by reaction condition).

350

351 **Table 2.** N and C bulk isotope enrichment factors (ε_N, ε_C)[a,b,c] and apparent kinetic isotope effects (^{15}N-AKIE,
352 ^{13}C-AKIE)[b,c] during the reduction of DNAN in different mineral systems.

System	ε_N (‰)	ε_C (‰)	^{15}N-AKIE (-)	^{13}C-AKIE (-)
Mackinawite				
Spike 1	-19 ± 1	-0.8 ± 0.6	1.039 ± 0.001	1.0008 ± 0.0008
ESHA	-16 ± 1	-0.7 ± 1.4	1.034 ± 0.001	1.0007 ± 0.0014
Spike 5	-16 ± 2	-1.5 ± 1.2	1.034 ± 0.002	1.0015 ± 0.0012
Average	-19 ± 2	-0.3 ± 0.6	1.039 ± 0.004	1.0003 ± 0.0006
Goethite				
Spike 1	-17 ± 3	-0.1 ± 0.3	1.035 ± 0.003	1.0000 ± 0.0003
ESHA	-16 ± 5	-0.6 ± 0.4	1.034 ± 0.005	1.0006 ± 0.0004
Spike 5	-11 ± 1	-1.2 ± 0.9	1.022 ± 0.001	1.0012 ± 0.0009
Average	-16 ± 3	-0.5 ± 0.3	1.033 ± 0.007	1.0005 ± 0.0003
Magnetite				
Spike 1	-15 ± 3	-0.7 ± 0.6	1.031 ± 0.003	1.0007 ± 0.0006
ESHA	-17 ± 3	-1.3 ± 0.2	1.036 ± 0.003	1.0013 ± 0.0005
Spike 5	-9 ± 2	-0.1 ± 0.2	1.018 ± 0.002	1.0000 ± 0.0002
Average	-17 ± 3	-0.3 ± 0.5	1.035 ± 0.006	1.0000 ± 0.0005
Alkaline Hydrolysis[d]	-2.7 ± 0.4	-6.0 ± 0.5	1.0027 ± 0.0004	1.0445 ± 0.0028
Enzymatic hydrolysis by O-demethylase[d]	-3.2 ± 0.1	-3.7 ± 0.1	1.0032 ± 0.0003	1.0269 ± 0.0053

[a]Values derived from log-linear regression analysis of eq. 1. [b]Uncertainties represent 95% confidence intervals. Averaged values according to the methods of Scott et al.[67] using the Pitman estimator. [d]Data from Ulrich et al.[42] [c]Obtained from previous work and references therein.[34,38–40,60]

Slight decreases in fractionation were observed during repeated contaminant exposure in Fe(II)/goethite and Fe(II)/magnetite systems (Table 2). This suggests that morphological changes (e.g., phase evolution and growth) occurring on the mineral structure during repeated surface oxidation and Fe(II) exposure may have limited the accessibility of reactive Fe(II) and thus slightly masked the isotope fractionation (Section S4.3, Figure S4). These changes were within experimental error of the initial spike experiment (ε_N = -17 ± 3‰ to -11 ± 1‰ and -15 ± 3‰ to -9 ± 2‰ between the single and multiple spike experiments for goethite and magnetite, respectively).

The collective C and N isotope fractionation data from all DNAN reduction experiments is plotted in Figure 3. Plots separated by mineral are in Figure S3. The values of $\delta^{15}N$ follow the general trend of ε_N values between -19 ± 1‰ to -9 ± 2‰ from individual DNAN reduction experiments. The scatter of $\delta^{15}N$ values illustrates that experimental and analytical uncertainties are larger in experiments with ESHA and after repeated spikes of DNAN. We conclude that those uncertainties are primarily responsible for the observed variations of ε_N values from the individual experiments as well as for the large confidence intervals (typically <0.5‰).[64] Based on this interpretation, we derived average ^{15}N-AKIE for DNAN reduction by each mineral, that is 1.039 ± 0.004, 1.033 ± 0.007, and 1.035 ± 0.005 for mackinawite, goethite, and magnetite, respectively (Table 2) which are again identical within uncertainty.

An analysis of eqs. 1 and 2 illustrates that a variation of ε_N for DNAN by ± 2.8‰, that is variations of ^{15}N-AKIE of ± 0.006 as observed in the average uncertainty of ^{15}N-AKIEs in this study, will introduce uncertainty in estimating the extent of transformation (i.e., $100 \times (1-c/c_0)$). This uncertainty will be higher when the observed N isotope fractionation is small (e.g., 15% for $\Delta^{15}N$ of 5‰) and level off as the N isotope fractionation increases (e.g., <7.5% at $\Delta^{15}N$ of 25‰[31]

see Figure 4). Given the large magnitude of ^{15}N-AKIEs observed here, the extent of DNAN reduction has to exceed only approximately 12% to generate N isotope fractionation beyond the typical total uncertainties of N isotope ratio measurements of ±1‰[33] based on an average ε_N value of –16‰.

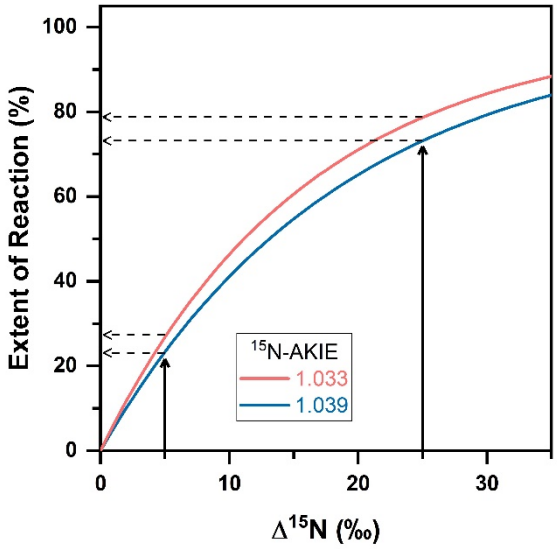

Figure 4. Changes in N isotope ratios ($\Delta^{15}N = \delta^{15}N - \delta^{15}N_0$) vs the extent of DNAN reaction ($100 \times (1-c/c_0)$). Equations 1 and 2 were used to illustrate variations in the extent of reaction given uncertainties in calculated AKIEs. Isotope fractionation profiles were generated using ε_N values of -16.0‰ (red) and -18.8‰ (blue), values typical for abiotic reductions of NACs but also within the range of isotope effects derived for the reduction of other NACs by other minerals. These ε_N values represent the extrema observed in this work. Dotted lines represent uncertainties in calculating the extent of reaction from uncertainties in ^{15}N–AKIEs.

The N isotope fractionation data for DNAN reduction reveal two important findings. First, abiotic reduction of DNAN will give rise to similar isotope enrichment factors across a variety of reaction conditions (i.e., regardless of the presence of NOM and previous contaminant exposures). Moreover, it is notable that ^{15}N-AKIE and ε_N values calculated in this study closely agree with those observed for the reduction of other model NACs by Fe-bearing mineral phases.[38-41] This comparison confirms our hypothesis that previous N isotope fractionation data for the abiotic reduction of NACs by Fe(II) bearing minerals can be extrapolated to new

contaminants such as DNAN. This observation also indicates that N isotope fractionation is a robust indicator for monitoring the extent of reduction of DNAN and other NACs in complex environmental matrices, even in the absence of knowledge relating to reaction kinetics and product formation. Indeed, this technique has previously been employed to provide quantitative estimates of the extent of organic contaminant transformations at contaminated field sites.[72] Our work, therefore, serves to qualify the prospective use of CSIA to assess the abiotic reduction of novel insensitive munitions in the environment.[31,73]

The combined C and N isotope analysis for DNAN reduction derived here is compared to the data for alkaline hydrolysis and aerobic biodegradation from Ulrich et al.[42] in Figure 5 and confirms that the different transformation pathways can also be discerned by CSIA. These data support the claim that N fractionation of DNAN during abiotic reduction is distinct from the isotopic fractionation observed in alkaline hydrolysis (nucleophilic aromatic substitution) and enzymatic hydrolysis (nucleophilic aliphatic substitution). Due to the vertical nature of the $\Lambda^{N/C}$ for the abiotic reduction data, a standard linear regression failed. Thus, the slope was found by plotting all of the $\Delta^{13}C$ vs $\Delta^{15}N$ data, finding the slope, and then taking the inverse of this value. The $\Lambda^{N/C}$ calculated via this method for abiotic reduction was 50.5 ± 23.2 (shown as the dotted line in Figure 5) in contrast to 0.46 ± 0.04 and 0.87 ± 0.18 for alkaline hydrolysis and biodegradation, respectively.[42] These results therefore suggest that an identification of those DNAN reaction pathways and their respective contributions in the environment would be possible.[74] Abiotic and biotic transformations of NACs typically elicit variable degree of ^{15}N, ^{13}C, and ^{2}H enrichment, [34,39,75] so that the observable isotope fractionation of processes occurring simultaneously can, in principle, be described by linear combinations of the enrichment factors pertinent to the individual, contributing processes.[52,74] Such dual or triple isotope analysis[31] can also

circumvent masking interferences, which so far, have been reported primarily for oxidative NAC degradation processes[76–78,32,75,79].

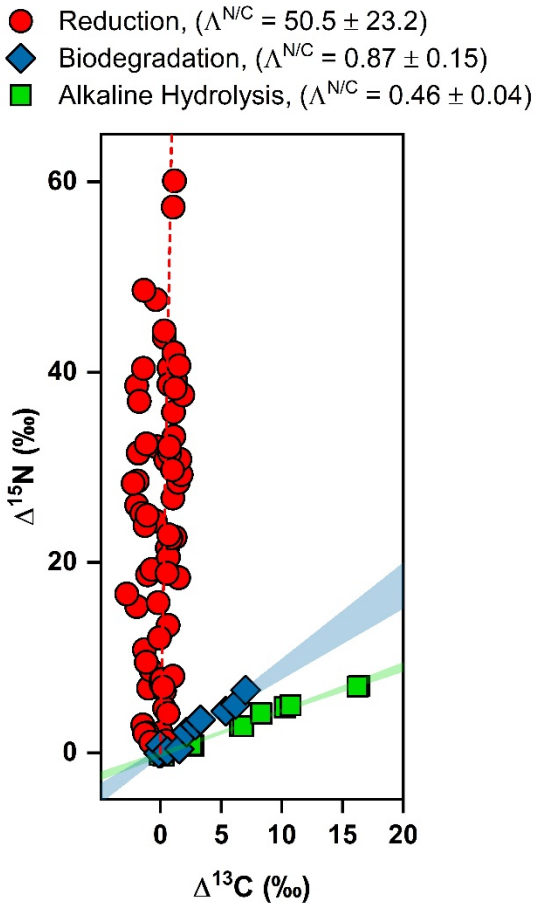

Figure 5. Two-dimensional isotope analysis for reductive and oxidative DNAN transformation pathways. Changes in $\delta^{13}C$ and $\delta^{15}N$ values were monitored during abiotic reduction (circles), alkaline hydrolysis (squares), and biodegradation (diamonds). Alkaline hydrolysis and biodegradation data were reproduced with permission from Ulrich et al.[42] Reduction data separated by mineral type are provided in Figure S5. The dotted line along the reduction data is provided simply to guide the eye. Moreover, any apparent inverse fractionation is an artifact of uncertainties in ^{13}C-AKIEs that are close to 1.

CONCLUSION

Knowledge of the stable isotope fractionation associated with DNAN reduction will allow for stakeholders to make quantitative estimates of the extent of DNAN degradation from measured $\delta^{15}N$ and $\delta^{13}C$ values of DNAN at contaminated sites. Our findings revealed that N and

C isotope fractionation during the mineral-mediated reduction of DNAN is consistent despite the presence of different minerals, NOM, and repeated contaminant exposures while remaining independent of reaction kinetics. The potential, changes of N isotope enrichment factors with repetitive exposure merit further investigation, especially considering that surface modification on natural minerals may be different than those for synthetic materials while those effects do not affect the interpretation of dual isotope analysis. Moreover, we showed that isotope fractionation during DNAN reduction will elicit $\Lambda^{N/C}$ values that are distinct from transformation pathways initiated by oxidation and substitution reactions.[38] By showing that our data reflects previous results for reductions of other NACs[30,33,34,36,38], this work illustrates how predictive comparisons can be made to assess the extent of pollutant transformation from existing data. Such practices provide a strengthened basis for CSIA to serve as a reliable tool for validating future remediation efforts.

ACKNOWLEDGEMENTS

This work was supported by the Strategic Environmental Research and Development Program (SERDP, Project No. ER2618). We thank Lee Penn (University of Minnesota) for providing access to XRD instrumentation. In addition, acknowledgments to the laboratories of Andreas Stein and Marc Hillmyer (University of Minnesota) for allowing the use of instrumentation for nitrogen adsorption analysis.

Funding Sources

This work was supported by the Strategic Environmental Research and Development Program (SERDP).

454

455 ASSOCIATED CONTENT

456 **Electronic Supplementary Information**

457 The following files are available free of charge via the internet at http://pubs.rsc.org/. A
458 detailed report of additional analytical methods, materials synthesis and characterization
459 techniques, batch reaction procedures, CSIA calculations, and further kinetics and isotope
460 results.

461

462 AUTHOR INFORMATION

463 **Author Contributions**

464 The manuscript was written through contributions of all authors. All authors have given
465 approval to the final version of the manuscript.

466

467 There are no competing interests.

468

469 REFERENCES

470 1 S. G. Dodard, M. Sarrazin, J. Hawari, L. Paquet, G. Ampleman, S. Thiboutot and G. I.
471 Sunahara, Ecotoxicological assessment of a high energetic and insensitive munitions
472 compound: 2,4-Dinitroanisole (DNAN), *J. Hazard. Mater.*, 2013, **262**, 143–150.

473 2 W. Trzcinski, S. Cudzilo, S. Dyjak and M. Nita, A comparison of the sensitivity and
474 performance characteristics of melt-pour explosives with TNT and DNAN binder, *Cent.*
475 *Eur. J. Energ. Mater.*, 2014, **11**, 443–455.

3 P. J. Davies and A. Provatas, *Characterization of 2,4-dinitroanisole: an ingredient for use in low sensitivity melt cast formulations*, DSTO-TR-1904, Edinburgh, South Australia, 2006, vol. DSTO-TR-19.

4 J. C. Spain, J. B. Hughes and H. Knackmuss, *Biodegradation of nitroaromatic compounds*, Lewis Publishers, Inc., Boca Raton, 2000.

5 R. D. Albright, *Cleanup of chemical and explosive munitions - locating, identifying contaminants, and planning for environmental remediation of land and sea military ranges and ordnance dumpsites*, William Andrew, Norwich, NY, USA, 2nd edn., 2012.

6 M. S. Johnson, W. S. Eck and E. M. Lent, Toxicity of Insensitive Munition (IMX) Formulations and Components, *Propellants, Explos. Pyrotech.*, 2017, **42**, 9–16.

7 V. M. Boddu, K. Abburi, S. W. Maloney and R. Damavarapu, Thermophysical properties of an insensitive munitions compound, 2,4-dinitroanisole, *J. Chem. Eng. Data*, 2008, **53**, 1120–1125.

8 L. Sviatenko, C. Kinney, L. Gorb, F. C. Hill, A. J. Bednar, S. Okovytyy and J. Leszczynski, Comprehensive investigations of kinetics of alkaline hydrolysis of TNT (2,4,6-trinitrotoluene), DNT (2,4-dinitrotoluene), and DNAN (2,4-dinitroanisole), *Environ. Sci. Technol.*, 2014, **48**, 10465–10474.

9 A. J. Salter-Blanc, E. J. Bylaska, J. J. Ritchie and P. G. Tratnyek, Mechanisms and kinetics of alkaline hydrolysis of the energetic nitroaromatic compounds 2,4,6-trinitrotoluene (TNT) and 2,4-dinitroanisole (DNAN), *Environ. Sci. Technol.*, 2013, **47**, 6790–6798.

10 H. W. Schroer, X. Li, H. J. Lehmler and C. L. Just, Metabolism and photolysis of 2,4-

497 dinitroanisole in Arabidopsis, *Environ. Sci. Technol.*, 2017, **51**, 13714–13722.

498 11 A. Halasz, J. Hawari and N. N. Perreault, New insights into the photochemical degradation
499 of the insensitive munition formulation IMX-101 in water, *Environ. Sci. Technol.*, 2018, **52**,
500 589–596.

501 12 S. C. Ahn, D. K. Cha, B. J. Kim and S.-Y. Oh, Detoxification of PAX-21 ammunitions
502 wastewater by zero-valent iron for microbial reduction of perchlorate, *J. Hazard. Mater.*,
503 2011, **192**, 909–914.

504 13 J. Hawari, F. Monteil-Rivera, N. N. Perreault, A. Halasz, L. Paquet, Z. Radovic-Hrapovic,
505 S. Deschamps, S. Thiboutot and G. Ampleman, Environmental fate of 2,4-dinitroanisole
506 (DNAN) and its reduced products, *Chemosphere*, 2015, **119**, 16–23.

507 14 J. Klausen, S. P. Troeber, S. B. Haderlein and R. P. Schwarzenbach, Reduction of
508 substituted nitrobenzenes by Fe(II) in aqueous mineral suspensions, *Environ. Sci. Technol.*,
509 1995, **29**, 2396–2404.

510 15 T. B. Hofstetter, C. G. Heijman, S. B. Haderlein, C. Holliger and R. P. Schwarzenbach,
511 Complete reduction of TNT and other (poly)nitroaromatic compounds under iron-reducing
512 subsurface conditions, *Environ. Sci. Technol.*, 1999, **33**, 1479–1487.

513 16 M. Elsner, R. P. Schwarzenbach and S. B. Haderlein, Reactivity of Fe(II)-bearing minerals
514 toward reductive transformation of organic contaminants, *Environ. Sci. Technol.*, 2004, **38**,
515 799–807.

516 17 D. Colón, E. J. Weber and J. L. Anderson, QSAR study of the reduction of nitroaromatics
517 by Fe(II) species, *Environ. Sci. Technol.*, 2006, **40**, 4976–4982.

518 18 F. H. Crocker, K. J. Indest and H. L. Fredrickson, Biodegradation of the cyclic nitramine
519 explosives RDX, HMX, and CL-20, *Appl. Microbiol. Biotechnol.*, 2006, **73**, 274–290.

520 19 P. Larese-Casanova and M. M. Scherer, Abiotic transformation of hexahydro-1,3,5-triazine
521 (RDX) by Green Rust, *Environ. Sci. Technol.*, 2008, **42**, 3795–3981.

522 20 C. Olivares, J. Liang, L. Abrell, R. Sierra-Alvarez and J. A. Field, Pathways of reductive
523 2,4-dinitroanisole (DNAN) biotransformation in sludge, *Biotechnol. Bioeng.*, 2013, **110**,
524 1595–1604.

525 21 J. B. Niedźwiecka and K. T. Finneran, Combined biological and abiotic reactions with iron
526 and Fe(III)-reducing microorganisms for remediation of explosives and insensitive
527 munitions (IM), *Environ. Sci. Water Res. Technol*, 2015, **1**, 34–39.

528 22 N. N. Perreault, D. Manno, A. Halasz, S. Thiboutot, G. Ampleman and J. Hawari, Aerobic
529 biotransformation of 2,4-dinitroanisole in soil and soil Bacillus sp., *Biodegradation*, 2012,
530 **23**, 287–295.

531 23 M. J. Kwon, E. J. O'Loughlin, D. A. Antonopoulos and K. T. Finneran, Geochemical and
532 microbiological processes contributing to the transformation of hexahydro-1,3,5-trinitro-
533 1,3,5-triazine (RDX) in contaminated aquifer material, *Chemosphere*, 2011, **84**, 1223–1230.

534 24 T. T. Fida, S. Palamuru, G. Pandey and J. C. Spain, Aerobic biodegradation of 2,4-
535 dinitroanisole by Nocardioides sp. strain JS1661, *Appl. Environ. Microbiol.*, 2014, **80**,
536 7725–7731.

537 25 J. B. Niedźwiecka, S. R. Drew, M. A. Schlautman, K. A. Millerick, E. Grubbs, N. Tharayil
538 and K. T. Finneran, Iron and electron shuttle mediated (bio)degradation of 2,4-

dinitroanisole (DNAN), *Environ. Sci. Technol.*, 2017, **51**, 10729–10735.

26 C. Olivares, R. Sierra-Alvarez, L. Abrell, J. Chorover, J. Field and R. Khatiwada, (Bio)transformation of 2,4-dinitroanisole (DNAN) in soils, *J. Hazard. Mater.*, 2016, **304**, 214–221.

27 S. E. Barrows, C. J. Cramer, D. G. Truhlar, M. S. Elovitz and E. J. Weber, Factors controlling regioselectivity in the reduction of polynitroaromatics in aqueous solution, *Environ. Sci. Technol.*, 1996, **30**, 3028–3038.

28 S. L. Larson, W. A. Martin, B. L. Escalon and M. Thompson, Dissolution, sorption, and kinetics involved in systems containing explosives, water, and soil, *Environ. Sci. Technol.*, 2008, **42**, 786–792.

29 B. R. Linker, R. Khatiwada, N. Pedrial, L. Abrell, R. Sierra, J. A. Field and J. Chorover, Adsorption of novel insensitive munitions comounds at clay mineral and metal oxide surfaces, *Environ. Chem.*, 2015, **12**, 74–84.

30 K. W. Weissmahr, M. Hildenbrand, R. P. Schwarzenbach and S. B. Haderlein, Laboratory and field scale evaluation of geochemical controls on groundwater transport of nitroaromatic ammunition residues, *Environ. Sci. Technol.*, 1999, **33**, 2593–2600.

31 R. S. Wijker, J. Bolotin, S. F. Nishino, J. C. Spain and T. B. Hofstetter, Using compound-specific isotope analysis to assess biodegradation of nitroaromatic explosives in the subsurface, *Environ. Sci. Technol.*, 2013, **47**, 6872–6883.

32 M. Elsner, Stable isotope fractionation to investigate natural transformation mechanisms of organic contaminants: principles, prospects and limitations., *J. Environ. Monit.*, 2010, **12**,

2005–31.

33 M. Elsner, M. A. Jochmann, T. B. Hofstetter, D. Hunkeler, A. Bernstein, T. C. Schmidt and A. Schimmelmann, Current challenges in compound-specific stable isotope analysis of environmental organic contaminants, *Anal. Bioanal. Chem.*, 2012, **403**, 2471–2491.

34 T. B. Hofstetter, P. Schwarzenbach and S. M. Bernasconi, Assessing transformation processes of organic compounds using stable isotope fractionation, *Environ. Sci. Technol.*, 2008, **42**, 7737–7743.

35 E. J. Weber, D. L. Spidle and K. A. Thorn, Covalent binding of aniline to humic substances. 1. Kinetic studies, *Environ. Sci. Technol.*, 1996, **30**, 2755–2763.

36 D. Colón, E. J. Weber and J. L. Anderson, Effect of natural organic matter on the reduction of nitroaromatics by Fe(II) species, *Environ. Sci. Technol.*, 2008, **42**, 6538–6543.

37 T. B. Hofstetter, J. Bolotin, S. G. Pati, M. Skarpeli-Liati, S. Spahr and R. S. Wijker, Isotope effects as new proxies for organic pollutant transformation, *Chim. Int. J. Chem.*, 2014, **68**, 788–792.

38 A. E. Hartenbach, T. B. Hofstetter, M. Aeschbacher, M. Sander, D. Kim, T. J. Strathmann, W. A. Arnold, C. J. Cramer and R. P. Schwarzenbach, Variability of nitrogen isotope fractionation during the reduction of nitroaromatic compounds with dissolved reductants, *Environ. Sci. Technol.*, 2008, **42**, 8352–8359.

39 A. Hartenbach, T. B. Hofstetter, M. Berg, J. Bolotin and R. P. Schwarzenbach, Using nitrogen isotope fractionation to assess abiotic reduction of nitroaromatic compounds, *Environ. Sci. Technol.*, 2006, **40**, 7710–7716.

40 T. B. Hofstetter, A. Neumann, W. A. Arnold, A. E. Hartenbach, J. Bolotin, C. J. Cramer and R. P. Schwarzenbach, Substituent effects on nitrogen isotope fractionation during abiotic reduction of nitroaromatic compounds, *Environ. Sci. Technol.*, 2008, **42**, 1997–2003.

41 C. A. Gorski, J. T. Nurmi, P. G. Tratnyek, T. B. Hofstetter and M. M. Scherer, Redox behavior of magnetite: implications for contaminant reduction, *Environ. Sci. Technol.*, 2010, **44**, 55–60.

42 B. A. Ulrich, M. Palatucci, J. Bolotin, J. C. Spain and T. B. Hofstetter, Different mechanisms of alkaline and enzymatic hydrolysis of the insensitive munition component 2,4-dinitroanisole lead to identical products, *Environ. Sci. Technol. Lett.*, 2018, **5**, 456–461.

43 N. B. Tobler, T. B. Hofstetter, K. L. Straub, D. Fontana and R. P. Schwarzenbach, Iron-mediated microbial oxidation and abiotic reduction of organic contaminants under anoxic conditions, *Environ. Sci. Technol.*, 2007, **41**, 7765–7772.

44 C. A. Gorski, R. Edwards, M. Sander, T. B. Hofstetter and S. M. Stewart, Thermodynamic characterization of iron oxide–aqueous Fe(II) redox couples, *Environ. Sci. Technol.*, 2016, **50**, 8538–8547.

45 S. M. Stewart, T. B. Hofstetter, P. Joshi and C. A. Gorski, Linking thermodynamics to pollutant reduction kinetics by Fe2+ bound toiron oxides, *Environ. Sci. Technol.*, 2018, **52**, 5600–5609.

46 E. E. Daugherty, B. Gilbert, P. S. Nico and T. Borch, Complexation and redox buffering of iron(II) by dissolved organic matter, *Environ. Sci. Technol.*, 2017, **51**, 11096–11104.

47 A. M. Vindedahl, J. H. Strehlau, W. A. Arnold and R. L. Penn, Organic matter and iron oxide nanoparticles: aggregation, interactions, and reactivity, *Environ. Sci. Nano*, 2016, **3**, 494–505.

48 A. M. Vindedahl, W. A. Arnold and R. L. Penn, Impact of Pahokee Peat humic acid and buffer identity on goethite aggregation and reactivity, *Environ. Sci. Nano*, 2015, **2**, 509–517.

49 A. M. Vindedahl, M. S. Stemig, W. A. Arnold and R. L. Penn, Character of humic substances as a predictor for goethite nanoparticle reactivity and aggregation, *Environ. Sci. Technol.*, 2016, **50**, 1200–1208.

50 J. H. Strehlau, M. S. Stemig, R. L. Penn and W. A. Arnold, Facet-dependent oxidative goethite growth as a function of aqueous solution conditions, *Environ. Sci. Technol.*, 2016, **50**, 10406–10412.

51 C. L. Chun, R. L. Penn and W. A. Arnold, Kinetic and microscopic studies of reductive transformations of organic contaminants on goethite, *Environ. Sci. Technol.*, 2006, **40**, 3299–3304.

52 T. B. Hofstetter, J. C. Spain, S. F. Nishino, J. Bolotin and R. P. Schwarzenbach, Identifying competing aerobic nitrobenzene biodegradation pathways by compound-specific isotope analysis, *Environ. Sci. Technol.*, 2008, **42**, 4764–4770.

53 R. S. Wijker, J. Zeyer and T. B. Hofstetter, Isotope fractionation associated with the simultaneous biodegradation of multiple nitrophenol isomers by Pseudomonas putida B2, *Environ. Sci. Process. Impacts*, 2017, **19**, 775–784.

54 E. C. Butler and K. F. Hayes, Effects of solution composition and pH on the reductive dechlorination of hexachloroethane by iron sulfide, *Environ. Sci. Technol.*, 1998, **32**, 1276–1284.

55 A. J. Anschutz and R. L. Penn, Reduction of crystalline iron(III) oxyhydroxides using hydroquinone: Influence of phase and particle size, *Geochem. Trans.*, 2005, **6**, 60–66.

56 U. Schwertmann and R. M. Cornell, in *Iron Oxides in the Laboratory: Preparation and Characterization*, Wiley-VCH Verlag GmbH, Weinheim, Germany, 2nd edn., 2000, pp. 135–140.

57 E. Viollier, P. W. Inglett, K. Hunter, A. N. Roychoudhury and P. Van Cappellen, The ferrozine method revisited: Fe(II)/Fe(III) determination in natural waters, *Appl. Geochemistry*, 2000, **15**, 785–790.

58 J. A. Bourdoiseau, M. Jeannin, C. Rémazeilles, R. Sabot and P. Refait, The transformation of mackinawite into greigite studied by Raman spectroscopy, *J. Raman Spectrosc.*, 2011, **42**, 496–504.

59 S. Brunauer, P. H. Emmett and E. Teller, Gases in multimolecular layers, *J. Am. Chem. Soc.*, 1938, **60**, 309–319.

60 M. Berg, J. Bolotin and T. B. Hofstetter, Compound-specific nitrogen and carbon isotope analysis of nitroaromatic compounds in aqueous samples using solid-phase microextraction coupled to GC/IRMS, *Anal. Chem.*, 2007, **79**, 2386–2393.

61 A. Kremser, M. A. Jochmann and T. C. Schmidt, PAL SPME Arrow - evaluation of a novel solid-phase microextraction device for freely dissolved PAHs in water, *Anal. Bioanal.*

Chem., 2016, **408**, 943–952.

62 S. Spahr, S. Huntscha, J. Bolotin, M. P. Maier, M. Elsner, J. Hollender and T. B. Hofstetter, Compound-specific isotope analysis of benzotriazole and its derivatives, *Anal. Bioanal. Chem*., 2013, **405**, 2843–2856.

63 S. Spahr, J. Bolotin, J. Schleucher, I. Ehlers, U. von Gunten and T. B. Hofstetter, Compound-specific carbon, nitrogen, and hydrogen isotope analysis of N -nitrosodimethylamine in aqueous solutions, *Anal. Chem*., 2015, **87**, 2916–2924.

64 S. G. Pati, H.-P. E. Kohler and T. B. Hofstetter, in *Methods in Enzymology*, Elsevier Inc., 1st edn., 2017, vol. 596, pp. 291–329.

65 R. U. Meckenstock, B. Morasch, C. Griebler and H. H. Richnow, Stable isotope fractionation analysis as a tool to monitor biodegradation in contaminated acquifers, *J. Contam. Hydrol*., 2004, **75**, 215–255.

66 M. Elsner, L. Zwank, D. Hunkeler and R. P. Schwarzenbach, A new concept linking observable stable isotope fractionation to transformation pathways of organic pollutants, *Environ. Sci. Technol*., 2005, **39**, 6896–6916.

67 K. M. Scott, X. Lu, C. M. Cavanaugh and J. S. Liu, Optimal methods for estimating kinetic isotope effects from different forms of the Rayleigh distillation equation, *Geochim. Cosmochim. Acta*, 2004, **68**, 433–442.

68 P. Zuman and B. Shah, Addition, reduction, and oxidation reactions of nitrosobenzene, *Chem. Rev*., 1994, **94**, 1621–1641.

69 G. C. Wallace, M. Sander, Y.-P. Chin and W. A. Arnold, Quantifying the electron donating capacities of sulfide and dissolved organic matter in sediment pore waters of wetlands, *Environ. Sci. Process. Impacts*, 2017, **19**, 758–767.

70 Y. Lan, A. S. Elwood Madden and E. C. Butler, Transformation of mackinawite to greigite by trichloroethylene and tetrachloroethylene, *Environ. Sci. Process. Impacts*, 2016, **00**, 1–8.

71 M. Tobiszewski and J. Namieśnik, Abiotic degradation of chlorinated ethanes and ethenes in water, *Environ. Sci. Pollut. Res.*, 2012, **19**, 1994–2006.

72 D. Hunkeler, R. U. Meckenstock, B. S. Lollar, T. C. Schmidt and J. T. Wilson, *A Guide for Assessing Biodegradation and Source Identification of Organic Ground Water Contaminants using Compound Specific Isotope Analysis (CSIA)*, Oklahoma, USA, 2008.

73 A. Bernstein, E. Adar, Z. Ronen, H. Lowag, W. Stichler and R. U. Meckenstock, Quantifying RDX biodegradation in groundwater using δ15N isotope analysis, *J. Contam. Hydrol.*, 2010, **111**, 25–35.

74 B. M. Van Breukelen, Extending the Rayleigh equation to allow competing isotope fractionating pathways to improve quantification of biodegradation, *Environ. Sci. Technol.*, 2007, **41**, 4004–4010.

75 N. B. Tobler and T. B. Hofstetter, Carbon and hydrogenisotope toluene oxidation by Geobacter metallireducens with different Fe(III) phases as terminal electron acceptors, *Environ. Sci. Technol.*, 2008, **42**, 7786–7792.

76 S. G. Pati, H. P. E. Kohler, J. Bolotin, R. E. Parales and T. B. Hofstetter, Isotope effects of

enzymatic dioxygenation of nitrobenzene and 2-nitrotoluene by nitrobenzene dioxygenase, *Environ. Sci. Technol.*, 2014, **48**, 10750–10759.

77 R. S. Wijker, S. G. Pati, J. Zeyer and T. B. Hofstetter, Enzyme kinetics of different types of flavin-dependent monooxygenases determine the observable contaminant stable isotope fractionation, *Environ. Sci. Technol. Lett.*, 2015, **2**, 329–334.

78 S. G. Pati, H.-P. E. Kohler, A. Pabis, P. Paneth, R. E. Parales and T. B. Hofstetter, Substrate and enzyme specificity of the kinetic isotope effects associated with the dioxygenation of nitroaromatic contaminants, *Environ. Sci. Technol.*, 2016, **50**, 6708–6716.

79 S. A. Mancini, S. K. Hirschorn, M. Elsner, G. Lacrampe-Couloume, B. E. Sleep, E. A. Edwards and B. Sherwood Lollar, Effects of trace element concentration on enzyme controlled stable isotope fractionation during aerobic biodegradation of toluene, *Environ. Sci. Technol.*, 2006, **40**, 7675–7681.